

Quantum walks on circles in phase space via superconducting circuit quantum electrodynamics

Peng Xue,¹ Barry C. Sanders,¹ Alexandre Blais,² and Kevin Lalumière²

¹*Institute for Quantum Information Science, University of Calgary, Alberta T2N 1N4, Canada*

²*Département de Physique et Regroupement Québécois sur les Matériaux de Pointe,
Université de Sherbrooke, Sherbrooke, Québec, Canada, J1K 2R1*

(Dated: February 6, 2020)

We show how a quantum walk can be implemented for the first time in a quantum quincunx created via superconducting circuit quantum electrodynamics (QED), and how interpolation from quantum to random walk is implemented by controllable decoherence using a two resonator system. Direct control over the coin qubit is difficult to achieve in either cavity or circuit QED, but we show that a Hadamard coin flip can be effected via direct driving of the cavity, with the result that the walker jumps between circles in phase space but still exhibits quantum walk behavior over 15 steps.

PACS numbers: 03.67.Ac, 42.50.Pq, 74.50.+r

The quantum walk (QW) is important in physics as a generalization of the ubiquitous random walk (RW), which underpins diffusion and Brownian motion. QWs are important in quantum algorithm research [1] because they exponentially speed up hitting time in glued tree graphs [2]. Although realization of a QW by a quantum quincunx, analogous to the quincunx (or Galton Board) for realizing the RW, has been proposed in ion traps [3] and cavity quantum electrodynamics (QED) [4, 5], the former requires cooling of ions to the center-of-mass motional ground state, and the latter hitting the atom with pulses that do not drive the cavity at all: these obstacles prevent quantum walks from being realized under foreseeable experimental conditions (a classical optical simulation of a quantum quincunx has been performed [6] but cannot be a proper QW without complementarity [7]).

Here we devise a quantum quincunx that can realize a QW in the laboratory for the first time by: (i) employing the Jaynes-Cummings model [8] to generalize the Hadamard transformation for coin flipping by directly driving the cavity rather than the atom; (ii) developing a theory of QWs on many circles in phase space (PS) rather than on a single circle as a consequence of generalizing the Hadamard transformation; (iii) optimizing the protocol by having the duration of the generalized Hadamard transformation depend on the time-dependent mean photon number in the cavity (with detailed theory to appear elsewhere [9]); (iv) implementing in a superconducting circuit QED (SCQED) system [10, 11] with a two-level Cooper Pair Box (CPB) serving as the quantum coin and a coplanar transmission line resonator with a single mode as the quantum walker; (v) introducing a double resonator scheme that can control decoherence while simultaneously enabling strong coupling between the CPB and the microwave field and permitting fast readout; and (vi) using the Holevo standard deviation as a measure of phase spreading and showing that the rate of spreading can be tuned by controllable decoherence to observe the quadratic enhancement of phase spreading for the QW vs RW.

In our scheme the QW is executed with indirect flipping of the coin via directly driving the cavity and allows controllable decoherence over circles in PS. Because the walker is directly driven rather than the coin, photon number is no longer conserved, and the walker jumps between circles in PS; however, a signature of quantum walking on circles in PS is evident in both the time-dependent phase distribution of the walker as well as via direct homodyne measurements to obtain the quadrature phase (QP) distribution for the walker. This signature is scaling of the standard deviation σ (which measures the walker's spreading) that is linear in time $\propto t$ for the QW, and whose power decreases with increasing decoherence until attaining the classical RW scaling $\propto \sqrt{t}$ for full decoherence. This controllable decoherence is achieved by introducing a second low- Q resonator to obtain fast readout [12].

To understand the QW in PS, it is helpful to first understand the RW in PS. The walker is a mode of the resonator, hence is equivalent to a harmonic oscillator, which can be described by its position x and momentum p . If the oscillator's energy $E \sim (\omega^2 x^2 + p^2)/2$ for unit mass and frequency ω , then the oscillator follows a periodic circular trajectory of radius \sqrt{E} in PS with physical oscillatory motion $x(t) = \sqrt{E} \cos \omega t$. This oscillator can be modified to execute a RW on a circle in PS by periodically applying an impulse that causes it to rotate either clockwise along the circle in PS by angle $\Delta\theta$ or counter-clockwise by the same amount, with the choice of $\pm\Delta\theta$ strictly random. If $\Delta\theta = 2\pi/d$, $d \in \mathbb{N}$, then the walker always remains on a (perhaps rotating) lattice on the circle with angular lattice spacing $\Delta\theta$. We refer to the coordinate in PS (x, p) as the walker's 'location' in PS, and the coin flip randomness that determine clockwise vs counter-clockwise angular steps implies that the walker's location is indeterminate hence described by a distribution $P(x, p)$.

In an *ideal* QW on a circle, the walker+coin state is a density operator $\rho \in \mathcal{B}(\mathcal{H})$ for $\mathcal{H} = \mathcal{H}_w \otimes \mathcal{H}_c$ (with walker space spanned by $d - 1$ discrete phase

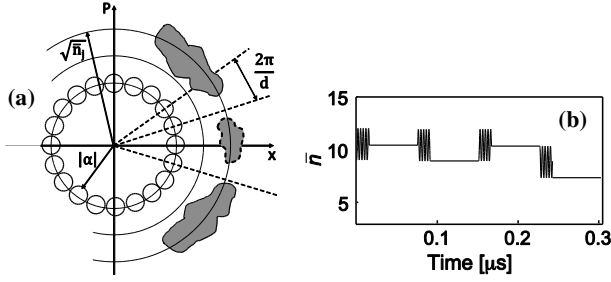


FIG. 1: (a) PS diagram depicting circles of fixed radius $\sqrt{\bar{n}_j}$ for circle j . The circle of radius $|\alpha|$ depicts $1/e$ contours of the Wigner function for coherent states separated by angular spacing $2\pi/d$ to make them distinct. A generic Wigner function $1/e$ contour (boundary of shaded areas) is depicted for circle j with mean $\langle \hat{n} \rangle = \bar{n}_j$. Solid boundaries represent contours around positive peaks, while dashed boundaries are for contours around negative peaks. (b) Average photon number \bar{n} vs evolution time t (μs) with period $(t_H^{(0)} + \tau)$.

states [3, 4], $\mathcal{H}_w = \text{span}\{|\theta_m = 2m\pi/d\rangle\}$ and coin space $\mathcal{H}_c = \text{span}\{|0\rangle, |1\rangle\}$, where $\mathcal{B}(\mathcal{H})$ is the Banach space of bounded operators on \mathcal{H} . The walker's phase distribution on the circle is

$$P_w(\theta) = \langle \theta | \rho_w | \theta \rangle / 2\pi, \quad \rho_w = \text{Tr}_c \rho, \quad (1)$$

with d equally spaced values of $\theta = \theta_m$. However, here the walker is following a circular trajectory in PS so the QW's Hilbert space is $\mathcal{H}_w = \text{span}\{|n\rangle; n \in \mathbb{N}\}$, with $|n\rangle$ a Fock state (\hat{n} eigenstate). Alternatively the generalized position representation $\{|x\rangle_\varphi\}$ can be used with $|x\rangle_\varphi$ an eigenstate of $\hat{x} \cos \varphi + \hat{p} \sin \varphi$, for \hat{x}, \hat{p} the canonical operators satisfying $[\hat{x}, \hat{p}] = i$ ($\hbar \equiv 1$). The QP distribution is $P_\varphi(x) = {}_\varphi\langle x | \rho_w | x \rangle_\varphi$ with φ the phase of a local oscillator. A convenient correspondence between the classical and quantum PS trajectory of the walker is provided by the Wigner quasiprobability distribution

$$W(x, p) = \int_{-\infty}^{\infty} \frac{dy}{2\pi} e^{ipy} \langle x - y/2 | \rho_w | x + y/2 \rangle \quad (2)$$

whose marginal distributions are $P_\varphi(x)$. Our scheme for realizing the first experimental QW builds on the cavity QED quantum quincunx [4], which alternately applies a coin flip Hadamard gate $H = |+\rangle\langle 0| + |-\rangle\langle 1|$, for $|\pm\rangle = (|0\rangle \pm |1\rangle)/\sqrt{2}$, followed by a rotation of the walker's state in PS by $\pm\Delta\theta$ with the sign depending on the coin state (with $\hat{n} = \hat{a}^\dagger \hat{a}$ for $\hat{a} = [\omega \hat{x} + i\hat{p}]/\sqrt{2\omega}$): $F = \exp(i\hat{n}\hat{\sigma}_z \Delta\theta)$. The initial state of the walker is a coherent state $|\alpha\rangle$: $\alpha \in \mathbb{R}$ and $\langle n | \alpha \rangle \equiv \sqrt{\bar{n}_0} = \sqrt{e^{-\bar{n}_0} \bar{n}_0^n / n!}$. Fig. 1 depicts PS, including how d is chosen given an initial walker state $|\alpha\rangle$ [4]: $\bar{n} + \sqrt{\bar{n}} < d < 2\pi\sqrt{\bar{n}}$. With this choice, the walker's angular step size is large enough to ensure enough distinguishability to yield a circular QW signature.

The simplicity of this model is rooted in the commutativity of $(FH)^N$ with \hat{n} , hence a constant of motion; thus

the walker's distance from the PS origin $\sqrt{\bar{n}}$ is fixed. Unfortunately alternating between F and H is not practical in SCQED. For the QW to be realized, and also to have controlled decoherence, a time-dependent driving field for the resonator is needed. As we see below, the sacrifice is that $[FH, \hat{n}] \neq 0$, but for realistic SCQED conditions, the QW on a circle is (surprisingly) evident provided that the step-by-step H pulse duration is judiciously chosen.

The goal is to observe the spreading of the QW's phase distribution, and the signature of the QW is that this spread is linear in time: specifically the standard deviation for the phase distribution satisfies $\sigma \propto t$ for the QW, whereas $\sigma \propto \sqrt{t}$ for the RW, and the QW can be tuned continuously from the RW by controlling decoherence. As phase is periodic, the usual root-mean-square approach to σ is problematic; instead we employ the Holevo standard deviation [13]

$$\sigma_H = \sqrt{| \langle e^{i\phi} \rangle |^{-2} - 1} \quad (3)$$

for $\langle e^{i\phi} \rangle = \int_0^{2\pi} d\phi P(\phi) e^{i\phi}$ with respect to any phase distribution $P(\phi)$ (1). The Holevo standard deviation is equivalent to the root-mean-square definition for small spreading on the circle, and σ_H naturally quantifies dispersion over all $\phi \in [0, 2\pi]$ [14]. Thus, for sufficiently short times (less than the time that phase distribution spreads over a significant fraction of the circle in PS), if the relation between phase spreading on the circle with time is a power law, then

$$\log \sigma_H = \zeta \log t + \xi \quad (4)$$

with $\zeta = 1$ for the QW and $\zeta = 1/2$ for the RW.

The SCQED Hamiltonian is [10]

$$\hat{H} = \hat{H}_{\text{JC}} + \hat{H}_d, \quad \hat{H}_d = \epsilon(t) (\hat{a}^\dagger e^{-i\omega_a t} + \hat{a} e^{i\omega_a t}) \quad (5)$$

for \hat{H}_d the time-dependent driving field Hamiltonian and $\hat{H}_{\text{JC}} = \omega_r \hat{n} + \omega_a \hat{\sigma}_z / 2 + g(\hat{a}^\dagger \hat{\sigma}_- + \hat{a} \hat{\sigma}_+)$ the Jaynes-Cummings (JC) Hamiltonian with ω_a and ω_r the coin and resonator frequencies, respectively, and g the coupling strength. It is sufficient to let $\epsilon(t)$ be a square wave so ϵ is a constant ($\epsilon = 0$ when the field is off). In the dispersive regime, $|\Delta| = |\omega_a - \omega_r| \gg g$, and in a frame rotating at ω_d for the qubit and the resonator, \hat{H} can be replaced by the effective Hamiltonian

$$\hat{H}_{\text{eff}} = g^2 \hat{n} \hat{\sigma}_z / \Delta - \delta_{\text{da}} \hat{\sigma}_z / 2 - \delta_{\text{dr}} \hat{n} + \Omega_R \hat{\sigma}_x / 2 + \epsilon(\hat{a}^\dagger + \hat{a}) \quad (6)$$

with $\delta_{\text{da}} = \omega_d - \omega_a$, $\delta_{\text{dr}} = \omega_d - \omega_r$, and $\Omega_R = 2g\epsilon/\delta_{\text{dr}}$ the Rabi frequency. The first term in the above expression effects the coin-induced walker phase shift. The atom transition is ac-Stark/Lamb shifted by $g^2 \hat{n} / \Delta$. To implement $\hat{H} = \exp[it_H \Omega_R \hat{\sigma}_x / 2]$ on the coin, we choose $\omega_d = 2\bar{n}g^2/\Delta - 2g\epsilon/\Delta + \omega_a$ with pulse duration $t_H = \pi/2\Omega_R$ and Ω_R a function of average photon number $\bar{n}(t) = \text{Tr}(\hat{n} \rho_w)$. The free evolution $\exp(-i\hat{H}_{\text{eff}} t)$ continues even when the driving field is off ($\epsilon = 0$). For

time τ between H -pulses, the walker steps through an angle $\Delta\theta \approx \pm g^2(\tau + t_H)/\Delta$.

Whereas the ideal QW conserves photon number, Eq. (6) violates this, which we interpret as the walker wandering between circles in PS. Circles have radii $\sqrt{\bar{n}(t)}$, and ω_d and t_H adjusted due to $\bar{n}(t)$ to ensure that the angular step size $\Delta\theta$ is constant regardless of how far the walker is from the PS origin. $\bar{n}(t)$ can be calculated as follows [9]. Begin by solving the Schrödinger equation $d|\varphi\rangle/dt = -i\hat{H}_{\text{eff}}|\varphi\rangle$ from time $t = 0$ to $t = N(t_H^{(0)} + \tau)$ with initial state $|\varphi_0\rangle = (|0\rangle + i|1\rangle)|\alpha\rangle/\sqrt{2}$, $t_H^{(0)} = \pi[\Delta + 2(|\alpha|^2 + 1)g^2/\Delta - 2g\epsilon/\Delta]/4g\epsilon$ and N the number of steps. Fig. 1(b) plots $\bar{n}(t)$ for $\alpha = 3$, $d = 21$ and typical system parameters $(\omega_a, \omega_r, g, \epsilon)/2\pi = (7000, 5000, 100, 1000)$ MHz. It is evident in the figure that the mean number oscillates and then settles down during the free evolution so the walker is concentrated on a circle of squared radius

$$\bar{n}_j = \left(t_H^{(0)} + \tau\right)^{-1} \int_{(j-1)(t_H^{(0)} + \tau)}^{j(t_H^{(0)} + \tau)} \bar{n}(t) dt \quad (7)$$

at step j . The corresponding Hadamard pulse duration $t_H^{(j)}$ for each step j is

$$t_H^{(j)} = \pi[\Delta + 2(\bar{n}_j + 1)g^2/\Delta - 2g\epsilon/\Delta]/4g\epsilon \quad (8)$$

for $j \in \mathbb{N}$, $\bar{n}_0 = 9$ and $t_H^{(0)} = 0.01567 \mu\text{s}$. Alternatively, to compensate for photon number fluctuations, it is possible to vary the frequency of the Hadamard pulse rather than its duration. For large step number N , the photon number distribution is approximately $P(n) = |\langle n | \rho_w | n \rangle|^2 \sim e^{-\bar{n}} \bar{n}^n / n!$ and the width of the photon number distribution $P(n)$ is $\delta n = \sqrt{\langle \hat{n}^2 \rangle - \langle \hat{n} \rangle^2} \approx \sqrt{\bar{n}}$: number spreading is thus negligible, and the walker can be regarded as indeed being concentrated locally in PS [9].

Coupling to additional uncontrollable degrees of freedom leads to energy relaxation and dephasing in the system. In the Born-Markov approximation, these effects can be characterized by a resonator photon leakage rate κ (determined at fabrication time by the resonator input and output coupling capacitances), an energy relaxation rate γ_1 , and a pure dephasing rate γ_ϕ for the qubit. The open system thus evolves according to

$$\dot{\rho} = -i[\hat{H}_{\text{eff}}, \rho] + \kappa \mathcal{D}[\hat{a}]\rho + \gamma_1 \mathcal{D}[\hat{\sigma}_-]\rho + (\gamma_\phi/2) \mathcal{D}[\hat{\sigma}_z]\rho, \quad (9)$$

with $\mathcal{D}[\hat{L}]\rho \equiv (2\hat{L}\rho\hat{L}^\dagger - \hat{L}^\dagger\hat{L}\rho - \rho\hat{L}^\dagger\hat{L})/2$. Relaxation and dephasing of a charge qubit in SCQED were reported in [11] as $T_1 = 7.3 \mu\text{s}$ and $T_2 = 500$ ns. These translate to $\gamma_1/2\pi = 0.02$ MHz and $\gamma_\phi/2\pi = (\gamma_2 - \gamma_1/2)/2\pi = 0.31$ MHz.

The master equation (9) is used to compute $\rho(t)$ from which the reduced state of the walker ρ_w is obtained and thence the phase distribution $P_w(\theta)$ (1). Empirically the phase distribution can be obtained by performing full optical homodyne tomography on the transmission line

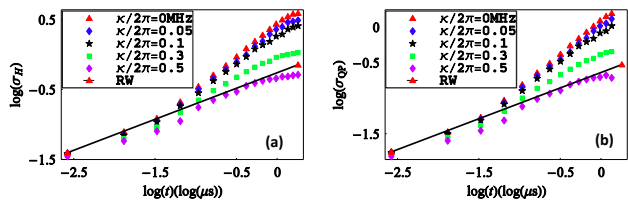


FIG. 2: Log-log plot of walker spread σ vs t (μs) for (a) phase distribution on the circle in PS and (b) QP distribution, for different κ and fixed $(g, \gamma_1, \gamma_\phi)/2\pi = (100, 0.02, 0.31)$ MHz.

$\kappa/2\pi$ (MHz)	s	Δs	$\log \sigma_H^0$	$\Delta \log \sigma_H^0$	r
0	0.924	0.009	0.442	0.004	0.990
0.05	0.879	0.013	0.362	0.006	0.991
0.1	0.822	0.014	0.279	0.008	0.992
0.3	0.615	0.022	-0.025	0.012	0.993
0.5	0.447	0.030	-0.309	0.017	0.990

$\kappa/2\pi$ (MHz)	s	Δs	$\log \sigma_{QP}^0$	$\Delta \log \sigma_{QP}^0$	r
0	0.937	0.006	0.093	0.004	0.988
0.05	0.892	0.009	0.016	0.006	0.989
0.1	0.832	0.013	-0.068	0.008	0.990
0.3	0.634	0.020	-0.372	0.012	0.993
0.5	0.453	0.034	-0.677	0.019	0.990

TABLE I: The linear regression data (a) $\log \sigma_H = (s \pm \Delta s) \log t + (\log \sigma_H^0 \pm \Delta \log \sigma_H^0)$ of the Holevo standard deviation of phase distribution and (b) $\log \sigma = (s \pm \Delta s) \log t + (\log \sigma_{QP}^0 \pm \Delta \log \sigma_{QP}^0)$ of the standard deviation of QP distribution in log-log scale for lossy cavities.

resonator to obtain $W(x, p)$ [17] from which $P_w(\theta)$ can be computed and $\sigma_H(t)$ thereby determined. The scaling of σ_H with t in Eq. (4) is a convenient empirical signature of the RW vs the QW.

As full tomography is expensive, it would be valuable to observe a QW directly from optical homodyne detection with a single choice of local oscillator phase φ instead of having to scan over many φ for full tomography. Our simulations show both $\sigma_H(t)$ for $P_w(\theta)$ and σ_{QP} for the QP distribution at $\varphi = 0$, with the choice of $\varphi = 0$ corresponding to having a local oscillator that is in phase with the walker at $t = 0$. For our choices of typical experimental parameters, the walker's phase distribution spreads from $-\pi$ to π on a scale of 15 steps so simulations are limited to fewer than 15 steps before the spreading effectively saturates and our comparison of the QW vs the RW breaks down.

Simulated evolution of $\sigma_H(t)$ and $\sigma_{QP}(t)$ are presented in Fig. 2(a,b), respectively. Corresponding linear regression data presented in Table I clearly reveals slopes compatible with the characteristic quadratic *decrease* in phase spreading for *increasing* decoherence of the QW until the transition to the RW [4].

These results show the significance of κ in decoherence from the QW to the RW. Moreover κ is much more important than γ_1 and γ_ϕ with respect to the scaling of $\sigma_{H, QP}$ with t . The pure dephasing rate γ_ϕ mainly leads

to smearing of the phase distribution and the phase distribution loses its symmetry. Furthermore, the effect of the energy relaxation rate γ_1 is small here compared with κ because of our choice of parameters.

Unfortunately κ must be low to obtain a quantum walk yet high to allow fast readout. This dilemma is resolved by instead using two modes [18]: one resonator (labeled a) of high-Q and acting as the walker and a second resonator (labeled b) of low-Q and used for fast readout [12]. The microwave radiation from resonator a is coupled into resonator b, and measurements ensue on resonator b. Measurements must be quick on the time scale of the walker's steps, so it cannot be longer than the time scale between pairs of Hadamard pulses. In the two-resonator system, κ_b has therefore a lower bound of $O(g^2/\Delta)$.

Due to coupling to resonator b, the transition frequency of the CPB in the resonator a and the pure dephasing rate are changing with the cavity field in resonator b, so the master equation for resonator a and the CPB is modified to [12]

$$\dot{\rho} = -i[\hat{H}_s, \rho] + \kappa_a \mathcal{D}[\hat{a}]\rho + \gamma_1 \mathcal{D}[\hat{\sigma}_-]\rho + \frac{\gamma_\varphi + \Gamma_m}{2} \mathcal{D}[\hat{\sigma}_z]\rho, \quad (10)$$

with

$$\hat{H}_s = \omega_a \hat{n} + \frac{\Omega'(t)}{2} \hat{\sigma}_z + [g \hat{a}^\dagger \hat{\sigma}_- + \epsilon(t) \hat{a}^\dagger e^{-i\omega_a t} + \text{hc}] \quad (11)$$

where $\Omega'(t) = \omega_a + 2\chi_b(|\alpha_b(t)|^2 + 1/2)$, and $\Gamma_m = 8|\chi_b||\alpha_b(t)|^2/\kappa_b$. In these expressions, χ_b is the cavity pull of the measurement resonator b and $\alpha_b(t)$ is the classical part of the measurement cavity field. Under these conditions, the master equation for the CPB and resonator b (10) is identical to Eq. (9) except for a parameter change. It is interesting to note that, in this two-resonator case, qubit dephasing can be tuned by changing the number of photons injected in the read-out resonator (corresponding to measurement-induced dephasing [10]). As a result, it should be possible to observe the crossover between the QW and the RW as a function of this tunable dephasing.

In summary we have introduced the following protocol to implement the QW on a circle in PS using SCQED. (i) Solve the Schrödinger equation numerically from $t = 0$ to $t = N(t_H^{(0)} + \tau)$, to obtain the mean photon number $\bar{n}(t)$ from which the sequence $\{\bar{n}_j\}$ and $\{t_H^{(j)}\}$ are obtained. (ii) Prepare a high-Q resonator in its vacuum

state (by simply cooling). (iii) When the vacuum state is prepared, inject a microwave field with a Gaussian pulse shape and temporal width ω_G in order to prepare the high-Q resonator in a coherent state $|\alpha\rangle$. (iv) After $t = 2\omega_G$, implement the Hadamard pulse on the CPB by injecting a square pulse of frequency ω_a into resonator b over time scale $t_H^{(j)}$ for step j . (v) Terminate the external driving of the resonator to allow free evolution over time scale τ . (vi) Repeat steps (iv) and (v) N times. (vii) Perform full tomography on resonator b by performing homodyne measurement over many values of ϕ and use standard inversion technique on the data.

In SCQED, the amplifier thermal noise is significant, with more thermal photons present than the mean resonator photon number [11]. However the signal QP distribution and full Wigner function can be obtained from the resultant homodyne detection statistics by convolving the readout with a thermal function (which is a Gaussian mixture of Gaussian states centered at the PS origin). The spread of the convolution is determined by the mean thermal photon number, which is typically 20. The result is expected to be noisy quadrature phase readout, but repetition will yield, on average, the desired linearity of $\log \sigma$ vs $\log t$. We can use a filter algorithm [19] which takes the inversion formula for the measured Radon transform of the Wigner function with thermal noise and reconstruct the Wigner function of the corresponding noiseless signal. Hence we can achieve the noiseless phase distribution and QP distribution with the Wigner function of the noiseless signal.

We have shown that the QW on a circle in PS can be implemented via SCQED with and without open systems effects using realistic parameters and find that the signature of the QW is evident under those conditions. Moreover full tomography may not be required because direct homodyne measurements over few quadratures reveal an unambiguous QW signature, and the RW can controllably emerge by tuning decoherence. Our scheme shows how a QW walk with just one walker can be implemented in a realistic system for the first time, and controllable decoherence can be performed thereby allowing continuous tunability between the quantum and classical regimes.

This work has been supported by NSERC, MITACS, CIFAR, FQRNT, QuantumWorks and iCORE. We thank Stephen Bartlett, Jay Gambetta, Steve Girvin, and Rob Schoelkopf for helpful discussions.

[1] D. Aharonov et al., Proc. 33rd ACM Symp. Theory of Comp., 50 (2001).
[2] A. M. Childs et al., Proc. 35th ACM Symp. on Theory of Comp., 59 (2003).
[3] B. C. Travaglione and G. J. Milburn, Phys. Rev. A **65**, 032310 (2002).

[4] B. C. Sanders et al., Phys. Rev. A **67**, 042305 (2003).
[5] T. Di, M. Hillery and M. S. Zubairy, Phys. Rev. A **70**, 032304 (2004).
[6] D. Bouwmeester et al., Phys. Rev. A **61**, 013410 (1999).
[7] V. Kendon and B. C. Sanders, Phys. Rev. A **71**, 022307 (2005).

- [8] E. T. Jaynes and F. W. Cummings, Proc. IEEE **51**, 89 (1963).
- [9] P. Xue and B. C. Sanders, unpublished.
- [10] A. Blais et al., Phys. Rev. A **69**, 062320 (2004).
- [11] A. Wallraff et al., Phys. Rev. Lett. **95**, 060501 (2005); A. Wallraff et al., Nature **413**, 162 (2004); D. I. Schuster et al., Phys. Rev. Lett. **94**, 123602 (2005).
- [12] R. J. Schoelkopf et al., private communication.
- [13] A. S. Holevo, Lecture Notes in Math. **1055** (Springer-Verlag, Berlin, 1984), p. 153.
- [14] H. M. Wiseman and R. B. Killip, Phys. Rev. A **56**, 944 (1997).
- [15] D. I. Schuster et al., Nature **445**, 515 (2007).
- [16] A. Blais et al., Phys. Rev. A **75**, 032329 (2007).
- [17] K. Vogel and H. Risken, Phys. Rev. A **40**, 2847 (1989).
- [18] H. M. Wiseman and G. J. Milburn, Phys. Rev. A **47**, 642 (1993).
- [19] S. Chountasis, L. K. Stergioulas, and A. Vourdas, J. Mod. Opt. **46**, 2131 (1999).